Rotationally Selected and Resolved State-to-State Photoelectron Study of Vanadium Monoxide Cation VO(+)(X(3)Σ(−); v(+) = 0−3)

ARTICLE *in* THE JOURNAL OF PHYSICAL CHEMISTRY A · OCTOBER 2015

Impact Factor: 2.69 · DOI: 10.1021/acs.jpca.5b09458

4 AUTHORS, INCLUDING:

C. Y. Ng

University of California, Davis

390 PUBLICATIONS **7,065** CITATIONS

SEE PROFILE

THE JOURNAL OF PHYSICAL CHEMISTRY A

Article

pubs.acs.org/JPCA

Rotationally Selected and Resolved State-to-State Photoelectron Study of Vanadium Monoxide Cation $VO^+(X^3\Sigma^-; v^+ = 0-3)$

Published as part of The Journal of Physical Chemistry A virtual special issue "Spectroscopy and Dynamics of Medium-Sized Molecules and Clusters: Theory, Experiment, and Applications".

Zhihong Luo,[†,‡] Yih-Chung Chang,[†] Huang Huang,[†] and C. Y. Ng*[,†]

[†]Department of Chemistry, University of California, Davis, California 95616, United States

[‡]Department of Physics, Tsinghua University, Beijing 100084, China

ABSTRACT: Vanadium monoxide cation $VO^+(X^3\Sigma^-)$ has been investigated by two-color visible (VIS)−ultraviolet (UV) pulsed field ionization−photoelectron (PFI−PE) methods. The unambiguous rotational assignment of rotationally selected and resolved VIS−UV−PFI−PE spectra thus obtained confirms the ground state term symmetry of VO^+ to be $X^3\Sigma^-$. The rotational analysis also yields the rotational constants $B_e^+ = 0.5716 \pm 0.0012$ cm^{-1} and $\alpha_e^+ = 0.0027 \pm 0.0005$ cm^{-1} for $VO^+(X^3\Sigma^-)$, from which the equilibrium bond distance of $VO^+(X^3\Sigma^-)$ is determined to be $r_e^+ = 1.557 \pm 0.002$ Å. This PFI−PE study covers the vibrational bands, $VO^+(X^3\Sigma^-; v^+ = 0, 1, 2,$ and $3) \leftarrow VO(X^4\Sigma^-; v'' = 0)$, which has made possible the determination of the vibrational constants for $VO^+(X^3\Sigma^-)$ to be $\omega_e^+ = 1068.0 \pm 0.7$ cm^{-1} and $\omega_e^+x_e^+ = 5.5 \pm 0.7$ cm^{-1}. The present state-to-state measurement also yields a more precise value (58 380.0 ± 0.7 cm^{-1} or 7.238 20 ± 0.000 09 eV) for the ionization energy of VO [IE(VO)]. This value along with the known IE(V) has allowed the determination of the difference between the 0 K bond dissociation energy (D_0) of $VO^+(X^3\Sigma^-)$ and that of $VO(X^4\Sigma^-)$ to be $D_0(V^+-O) - D_0(V-O) = IE(V) - IE(VO) = -3967 \pm 1$ cm^{-1}.

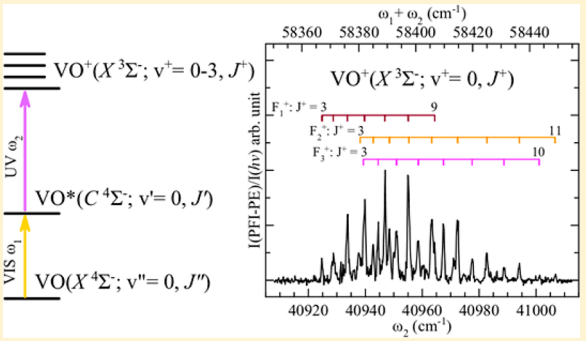

I. INTRODUCTION

Vanadium monoxide (VO) and its cation (VO^+) are important astronomical species. Their presence in astronomical environments is manifested in the spectroscopy of cool M-stars.[1] The majority of previous experimental and theoretical efforts have been devoted to the study of neutral VO.[2−14] The early He I photoelectron study of VO^+ cation was conducted by Dyke et al., yielding a value of 7.25 ± 0.01 eV for the ionization energy (IE) of VO and the term symmetry of $^3\Sigma^-$ for $VO^+(X)$ cationic ground state. In addition, the He I study also provided a value of 5.98 ± 0.10 eV for the 0 K bond dissociation energy of $VO^+(X^3\Sigma^-)$ [$D_0(V^+-O)$].[3] The latter value was found to agree with the value of $D_0(V^+-O) = 5.81 \pm 0.17$ eV deduced in a guided ion beam experiment.[6] The most detailed spectroscopic study of $VO^+(X^3\Sigma)$ was conducted by Harrington and Weisshaar by employing a two-color visible (VIS)−ultraviolet (UV) excitation scheme along with the high resolution pulsed field ionization−photoelectron (PFI−PE) detection method, resulting in the determination of a highly precise IE(VO) value of 58 383 ± 5 cm^{-1} along with spectroscopic constants for $VO^+(X^3\Sigma^-; v^+ = 0)$ ground state.[7] Constrained by the low sensitivity of these PFI−PE experiments, the majority of previous PFI−PE measurements have been limited to the study of molecular ground states. In the present study, we report a two-color VIS−UV−PFI−PE study, which covers the $v^+ = 0-3$ vibrational states of $VO^+(X^3\Sigma^-)$. In addition to confirming the $^3\Sigma^-$ symmetry assignment for $VO^+(X)$ and providing more precise values for the IE(VO) and rotational constants of $VO^+(X^3\Sigma^-; v^+ = 0)$, we have also determined new rotational and vibrational constants for the vibrationally excited $VO^+(X^3\Sigma^-; v^+ = 1-3)$ states.

In the past few years, we have devoted considerable effort to acquiring precise energetic and spectroscopic data of transition-metal (M)-containing diatomic species MX and their cations MX^+, where M = 3d and 4d transition metal elements, such as Ti, V, Fe, Co, Ni, Zr, Nb, and Mo, and X = main group elements, such as X = C, O, and N. By using the two-color VIS−UV−PFI−PE detection techniques, we have been able to perform rotationally selected and resolved state-to-state photoelectron studies on selected MX/MX^+ systems.[15−24] Recently, we have extended the high resolution PFI−PE studies to measurements of triatomic species, such as methylidyne radical (VCH)[25] and titanium dioxide (TiO_2).[26] Highly precise and reliable energetic and spectroscopic data obtained in these experiments have been used to benchmark theoretical predictions based on state-of-the-art *ab initio*

Received: September 28, 2015
Revised: October 20, 2015

DOI: 10.1021/acs.jpca.5b09458
J. Phys. Chem. A XXXX, XXX, XXX−XXX

quantum calculations.[23,27−29] A main goal is to identify a practical *ab initio* quantum computation procedure that can provide reliable energetic as well as spectroscopic predictions for transition metal-containing species with chemical accuracy (≈30−50 meV). The present rotationally resolved PFI−PE experiment represents a continuing quest toward this goal.

II. EXPERIMENT

The arrangement of the photoion−photoelectron apparatus and procedures used in this experiment are similar to those described in detail previously.[15,19] The apparatus consists of a laser ablation beam source for the generation of supersonically cooled VO molecules, a time-of-flight (TOF) mass spectrometer for photoion detection, and a TOF photoelectron spectrometer for PFI−PE detection. Two independently tunable dye lasers, a Lamba-Physics Model: FL2002 dye laser [optical bandwidth = 0.4 cm^{-1} (full-width at half-maximum, fwhm)] and a Lamba-Physics FL3002 dye laser [optical bandwidth = 0.2 cm^{-1} (fwhm)] pumped by the same Nd:YAG laser (Spectra-Physics Model: PRO-290; repetition rate = 30 Hz) were employed to generate the respective VIS ω_1 and UV ω_2 dye laser outputs as required by the experiment.

The VO molecules were generated by reactions between gaseous V atoms and O_2 molecules. The gaseous V atoms were produced by laser ablation of a translating and rotating solid V rod (99% purity) using the frequency-doubled 532 nm output (pulse energy = 2 mJ) of a Nd:YAG laser operated at 30 Hz, in the presence of an O_2/He mixture (O_2/He < 1%), which was introduced into the reaction region of the laser ablation source by a pulsed valve (repetition rate = 30 Hz; total stagnation pressure of the O_2/He mixture used = 40 psi). The VO sample was allowed to undergo supersonic expansion through a capillary before passing through a conical skimmer to enter the photoionization/photoextraction (PI/PEX) region, where it intersected with the VIS ω_1 and UV ω_2 laser beams. Here, excited VO molecules in one or two rovibronically selected excited intermediate states were prepared by VIS ω_1 excitation prior to UV ω_2 photoionization.

The photoions formed in the PI/PEX region were guided into the TOF mass spectrometer by a dc extraction electric field. For the present PFI−PE study, a pulsing scheme was employed. Briefly, the PI/PEX region was kept field free during the laser excitation to minimize the decay of high-n Rydberg states. A small pulse field (amplitude = 0.1 V/cm, pulse width = 2 μs) was applied at the PI/PEX region to disperse prompt background electrons at 200 ns delay with respect to the UV ω_2 pulse. At a delay of 2.2 μs with respect to the UV ω_2 pulse, a PFI pulse (pulse amplitude = 0.6 V/cm, pulse width = 10 μs) was applied to the PI/PEX region to field ionize the high-n Rydberg molecules and guide the resulting PFI−PEs into the TOF photoelectron spectrometer for detection. All energetic data presented here have been corrected for the Stark shift induced by the pulse fields.[17] All spectra represent the averages of at least three reproducible scans.

III. RESULTS AND DISCUSSION

Figure 1 depicts the VO*($C^4\Sigma^-$; v′ = 0) ← VO ($X^4\Sigma^-$; v″ = 0) excitation band obtained by scanning VIS ω_1 in the range of 17 387−17 450 cm^{-1} and fixing UV ω_2 at 41 516.76 cm^{-1}, where VO* represents the VIS ω_1 excited intermediate in a VO*($C^4\Sigma^-$; v′ = 0, J') state. The effective Hamiltonian for the $^4\Sigma^-$ states is shown in eq 1.

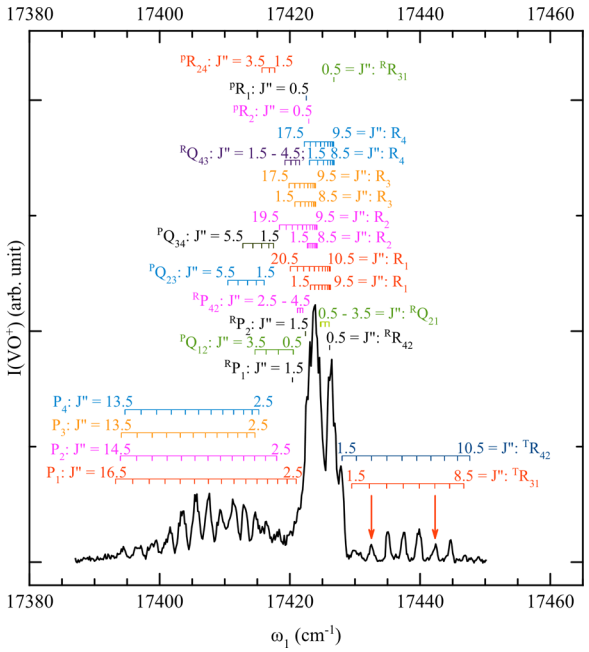

Figure 1. VO*($C^4\Sigma^-$; v′ = 0) ← VO($X^4\Sigma^-$; v″ = 0) excitation band obtained by scanning VIS ω_1 in the range 17 387−17 450 cm^{-1} and fixing UV ω_2 at 41 516.76 cm^{-1}. Thus, only VO*($C^4\Sigma^-$; v′ = 0, J') molecules excited by VIS ω_1 can be photoionization by UV ω_2. Simulation based on the effective Hamiltonian of eq 1 shows that the spectrum consists of 23 rotational branches, P_1, P_2, P_3, P_4, $^RP_1$, $^RP_2$, $^RP_{42}$, $^PQ_{12}$, $^PQ_{23}$, $^PQ_{34}$, $^RQ_{21}$, $^RQ_{43}$, R_1, R_2, R_3, R_4, $^PR_1$, $^PR_2$, $^PR_{24}$, $^RR_{31}$, $^RR_{42}$, $^TR_{31}$, and $^TR_{42}$, as marked on top of the spectrum. Two rotational excitation peaks located at 17 432.54 and 17 442.27 cm^{-1} (marked by downward pointing red arrows) were chosen for VIS−UV−PFI−PE measurements.

$$H_{\text{eff}} = B\mathbf{N}^2 + (2/3)\lambda(3\mathbf{S}_z^2 - \mathbf{S}^2) + \gamma\mathbf{N}\cdot\mathbf{S} \quad (1)$$

Here, B is the rotational constant, λ is the spin−spin coupling constant, and γ is the spin−orbital coupling constant, and $\mathbf{N}$ and $\mathbf{S}$ are the angular momenta of the core rotation and the electron spin, respectively. According to the convention of Herzberg, J is the total angular momentum, which has the values of $J = N + 3/2$ (F_1), $J = N + 1/2$ (F_2), $J = N - 1/2$ (F_3), and $J = N - 3/2$ (F_4). By using the spectroscopic constants obtained from the work of Cheung et al.[2] and the pgopher software,[30] we have simulated the excitation band on the basis of the effective Hamiltonian of eq 1. The simulation indicates that this excitation band consists of twenty-three rotational branches, P_1, P_2, P_3, P_4, $^RP_1$, $^RP_2$, $^RP_{42}$, $^PQ_{12}$, $^PQ_{23}$, $^PQ_{34}$, $^RQ_{21}$, $^RQ_{43}$, R_1, R_2, R_3, R_4, $^PR_1$, $^PR_2$, $^PR_{24}$, $^RR_{31}$, $^RR_{42}$, $^TR_{31}$, and $^TR_{42}$, as marked on top of the spectrum shown in Figure 1. Limited by the optical bandwidth of the VIS ω_1 and UV ω_2 lasers used, many excitation peaks resolved in the spectrum of Figure 1 consist of multiple rotational transitions. After a careful examination of the experimental and simulated spectra, we have selected two rotational excitation peaks located at 17 432.54 and 17 442.27 cm^{-1} (marked by downward pointing red arrows in Figure 1) for VIS−UV−PFI−PE measurements. The peak at VIS ω_1 = 17 432.54 cm^{-1} composed of the $^TR_{31}(2.5)$ and $^TR_{42}(3.5)$ rotational transitions. The peak at VIS ω_1 = 17 442.27 cm^{-1} is contributed predominantly by the $^TR_{31}(6.5)$ rotational transition. In the previous VIS−UV−PFI−PE study of Harrington and Weisshaar,[7] a different excitation vibronic band VO*($C^4\Sigma^-$; v′ = 3) ← VO($X^4\Sigma^-$; v″ = 0) was

DOI: 10.1021/acs.jpca.5b09458
J. Phys. Chem. A XXXX, XXX, XXX−XXX

used to prepare the intermediate excited VO*($C^4\Sigma^-$; v′ = 3, J') state for the UV ω_2 photoionization study.

A. VIS−UV−PFI−PE Spectra for $VO^+(X^3\Sigma^-; v^+ = 0, J^+)$. The IE(VO) value determined previously was helpful in narrowing down the energy range for performing PFI−PE measurements in the present study. The top black spectra shown in Figures 2 and 3 are the VIS−UV−PFI−PE spectra for

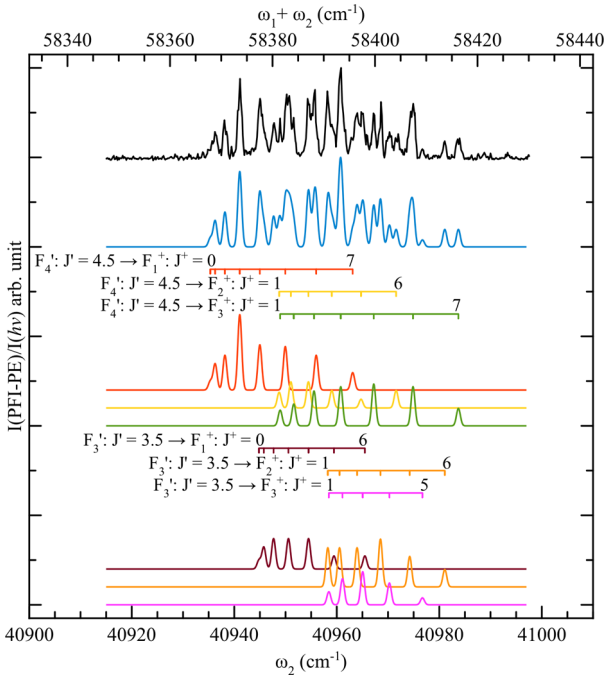

Figure 2. VIS−UV−PFI−PE spectrum for $VO^+(X^3\Sigma^-; v^+ = 0, J^+)$ (top black curve) obtained by setting ω_1 = 17 432.54 cm^{-1} and scanning ω_2 in the range 40 915−40 997 cm^{-1}. At VIS ω_1 = 17 432.54 cm^{-1}, the $^TR_{31}(2.5)$ and $^TR_{42}(3.5)$ transition lines of the VO*($C^4\Sigma^-$; v′ = 0) ← VO($X^4\Sigma^-$; v″ = 0) band are excited, resulting in populating the VO*[$C^4\Sigma^-$; v′ = 0, $F_3'(J' = 3.5)$ and $F_4'(J' = 4.5)$] levels, respectively. The blue curve is the sum of individual simulated spectra for the six transition series, $VO^+[X^3\Sigma^-; v^+ = 0, F_i^+(J^+)$ $(i = 1-3)]$ ← VO*[$C^4\Sigma^-$; v′ = 0, $F_3'(J' = 3.5)$ and $F_4'(J' = 4.5)$], which are shown as the brown, orange, purple, red, yellow, and green curves, respectively.

$VO^+(X^3\Sigma^-; v^+ = 0, J^+)$ obtained by setting VIS ω_1 at 17 432.54 and 17 442.27 cm^{-1} and scanning UV ω_2 in the ranges 40 915−40 997 and 40 908−41 012 cm^{-1}, respectively. Because setting VIS ω_1 = 17 432.54 cm^{-1} corresponds to exciting the $^TR_{31}(2.5)$ and $^TR_{42}(3.5)$ rotational transitions of the VO*($C^4\Sigma^-$; v′ = 0) ← VO($X^4\Sigma^-$; v″ = 0) band, the spectrum of Figure 2 is obtained by preparing the excited VO molecules in the VO*[$C^4\Sigma^-$; v′ = 0, $F_3(J' = 3.5)$ and $F_4(J' = 4.5)$] rovibronic states. In Figure 3, the VIS−UV−PFI−PE spectrum for $VO^+(X^3\Sigma^-; v^+ = 0, J^+)$ is obtained by exciting the $^TR_{31}(6.5)$ rotational transition, that is, by preparing excited VO molecules in the VO*[$C^4\Sigma^-$; v′ = 0, $F_3(J' = 7.5)$] rovibronic level prior to UV ω_2 photoionization.

The $VO^+(X^3\Sigma^-)$ ground state belongs to the Hund's case (b) coupling scheme, and the effective Hamiltonian for this state is the same as the neutral VO($X^4\Sigma^-$) state. The total angular momentum J^+ of $VO^+(X^3\Sigma^-)$ has three values $J^+ = N^+ + 1(F_1^+)$, $J^+ = N^+(F_2^+)$, $J^+ = N^+ - 1(F_3^+)$. By using the pgopher software[30] and the spectroscopic constants[2] for the VO($X^4\Sigma^-$) ground state obtained from the work of Cheung et al., we have analyzed and simulated the VIS−UV−PFI−PE spectra of

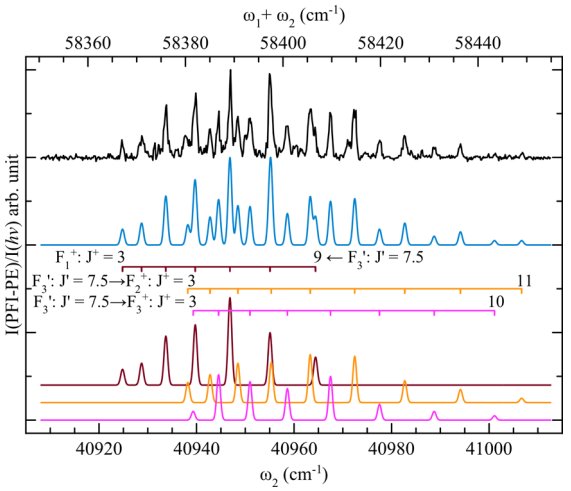

Figure 3. VIS−UV−PFI−PE spectrum for $VO^+(X^3\Sigma^-; v^+ = 0, J^+)$ (top black curve) obtained by setting VIS ω_1 = 17 442.27 cm^{-1} and scanning UV ω_2 in the range 40 908−41 012 cm^{-1}. At VIS ω_1 = 17 442.27 cm^{-1}, only the $^TR_{31}(6.5)$ transition of the VO*($C^4\Sigma^-$; v′ = 0) ← VO($X^4\Sigma^-$; v″ = 0) band is excited, resulting in the populating of the VO*[$C^4\Sigma^-$; v′ = 0, $F_3'(J' = 7.5)$] level. The blue curve is the sum of individual simulations of the transition series, $VO^+[X^3\Sigma^-; v^+ = 0, F_i^+(J^+)$ $(i = 1-3)]$ ← VO*[$C^4\Sigma^-$; v′ = 0, $F_3'(J' = 7.5)$], which are shown as the brown, orange, and purple curves, respectively.

Figures 2 and 3, giving the spectroscopic constants for the cationic ground state: ν_{00}^+ = 58 384.8 ± 0.7 cm^{-1}, B_0^+ = 0.5705 ± 0.0005 cm^{-1}, λ_0^+ = 6.701 ± 0.025 cm^{-1}, and γ_0^+ = 0.0345 ± 0.0047 cm^{-1}. The band origin $\nu_{00}^+ = \Delta T_{e^+e''} + G(v^+ = 0) - G(v'' = 0)$, where $\Delta T_{e^+e''}$ is the energy difference between the minima of the ionic and neutral ground potential curves and $G(v^+ = 0)$ and $G(v'' = 0)$ are the vibration energies of the respective ionic and neutral ground states. The bond length for $VO^+(X^3\Sigma^-; v^+ = 0)$ is derived from the measured rotational constant B_0^+ to be r_0^+ = 1.558 ± 0.001 Å. These spectroscopic data obtained for $VO^+(X^3\Sigma^-; v^+ = 0)$ are listed in Table 1 for comparison with those reported previously by Harrington and Weisshaar. Taking into account experimental uncertainties, the results of the present and previous experiments are in agreement. However, the error limits achieved in this study are smaller than those reported in ref 7.

Because the spectrum in Figure 2 involves the contributions of two rotational levels excited at VIS ω_1 = 17432.54 cm^{-1}, the spectrum consists of six series of rotational PFI−PE transitions. The three simulated spectra for the rotational transition series, $VO^+[X^3\Sigma^-; v^+ = 0, F_i^+(J^+)$ $(i = 1-3)]$ ← VO*[$C^4\Sigma^-$; v′ = 0, $F_3'(J' = 3.5)$], were shown in the figure as the brown, orange, and purple curves, respectively (bottom set of simulated spectra). The J^+ states are found to be in the ranges 0−6 for F_1^+, 1−6 for F_2^+, and 1−5 for F_3^+. Similarly, the simulated spectra for the three transition series, $VO^+[X^3\Sigma^-; v^+ = 0, F_i^+(J^+)$ $(i = 1-3)]$ ← VO*[$C^4\Sigma^-$; v′ = 0, $F_4'(J'= 4.5)$] were also shown in Figure 2 as the red, yellow, and green curves, respectively (second to the bottom set of simulated spectra), revealing that the J^+ states are formed in the ranges 0−7 for F_1^+, 1−6 for F_2^+, and 1−7 for F_3^+. The assignments of the observed $F_i^+(J^+)$ levels are also marked on top of individual simulated spectra in the figure with the corresponding color codes. Similar to previous studies, all simulated spectra for the PFI−PE rotational transitions assumed a Gaussian instrumental profile of fwhm = 0.9 cm^{-1} for the energy bandwidth of PFI−PE detection. The

DOI: 10.1021/acs.jpca.5b09458
J. Phys. Chem. A XXXX, XXX, XXX−XXX

Table 1. Spectroscopic Constants and Energetic Data of $VO^+(X\ ^3\Sigma^-;\ v^+ = 0, 1, 2, \text{and } 3)$[a]

	X $^3\Sigma^-$			
	$v^+ = 0$	$v^+ = 1$	$v^+ = 2$	$v^+ = 3$
ν^+_{v0} (cm^{-1})	58384.8 ± 0.7	59441.8 ± 0.7	60487.7 ± 0.7	61522.7 ± 0.7
IE	58380.0 ± 0.7			
	58383 ± 5[b]			
B_v^+ (cm^{-1})	0.5705 ± 0.0005	0.5680 ± 0.0007	0.5636 ± 0.0007	0.5631 ± 0.0008
	0.5682 ± 0.0016[b]			
λ_v^+ (cm^{-1})	6.701 ± 0.025	6.702 ± 0.034	6.690 ± 0.035	6.675 ± 0.038
	6.61 ± 0.10[b]			
γ_v^+ (cm^{-1})	0.0345 ± 0.0047	0.0303 ± 0.0059	0.0293 ± 0.0065	0.0209 ± 0.0082
	0.018 ± 0.014[b]			
r_v^+ (Å)	1.558 ± 0.001	1.561 ± 0.001	1.568 ± 0.001	1.568 ± 0.001
	1.5612 ± 0.0022[b]			
Vibrational Constant				
$\Delta G(1/2)$ (cm^{-1})	1057.0 ± 0.7			
$\Delta G(3/2)$ (cm^{-1})	1045.9 ± 0.7			
$\Delta G(5/2)$ (cm^{-1})	1035.0 ± 0.7			
ω_e^+ (cm^{-1})	1068.0 ± 0.7			
$\omega_e^+ x_e^+$ (cm^{-1})	5.5 ± 0.7			
Rotation Constant				
B_e^+ (cm^{-1})	0.5716 ± 0.0012			
α_e^+ (cm^{-1})	0.0027 ± 0.0005			
r_e^+ (Å)	1.557 ± 0.002			
Difference in Dissociation Energies				
$D_0(V^+{-}O) - D_0(V{-}O) = IE(V) - IE(VO)$	−3967 ± 1 cm^{-1}			

[a]This work. [b]Reference 7.

heights of individual rotational transitions of the simulated spectrum are scaled to give the best fits to the experimental spectrum. The blue curve (shown below the PFI−PE spectrum) is the overall simulated curve, which represents the sum of individual simulated curves for the rotational series. The excellent fits obtained together with the observation of $J^+ = 0$ in $F_1^+(J^+)$, and $J^+ = 1$ in $F_2^+(J^+)$ and $F_3^+(J^+)$ are unambiguous evidence for the term symmetry assignment of $^3\Sigma^-$ for the $VO^+(X)$ ground state. The VIS−UV−PFI−PE spectrum of Figure 3 consists of three PFI−PE rotational transition series of $VO^+[X^3\Sigma^-;\ v^+ = 0, F_i^+(J^+)\ (i = 1{-}3)] \leftarrow VO^*[C^4\Sigma^-;\ v' = 0, F_3'(J' = 7.5)]$. The corresponding simulated spectra for the observed three rotational series are shown in Figure 3 as the brown, orange, and purple curves. As shown in Figure 3, the J^+ states are observed to be in ranges $J^+ = 3{-}9$, $3{-}11$, and $3{-}10$ for the F_1^+, F_2^+, and F_3^+ series, respectively.

The J^+-rotational peaks of simulated spectra for the rotational transition series shown in Figures 2 and 3 exhibit $\Delta J^+ = J^+ - J'$ transitions in the range within ±5 or $|\Delta J^+| \leq 5$, which are similar to that found in previous VIS−UV−PFI−PE studies of VC/VC^+, VN/VN^+, TiO/TiO^+, and FeC/FeC^+.[15,18,19,23] The change of rotational angular momentum of the ion core, and thus the $|\Delta J^+|$ change in a photoionization process, can be viewed to result from the scattering of the outgoing photoelectron with the ion core. The energy transfer between the photoelectron and the ion core rotation represent a breakdown of the Born−Oppenheimer approximation, and thus the formation of a J^+-rotational state with a smaller $|\Delta J^+|$ change is favored. The intensity pattern of $|\Delta J^+|$ transitions for a rotational transition series observed here, which exhibits the highest intensity at $|\Delta J^+|$ close to zero and decreases as $|\Delta J^+|$ is increased, is a normal appearance, and has been observed in many MX/MX^+ as well as the CH_3Br/CH_3Br^+ and CH_3I/CH_3I^+ photoionization systems.[31,32] The range of $|\Delta J^+|$ changes was found to depend on the rotational constant or the density of states of the molecular species involved. For molecular species with smaller rotational constants, such as MoO/MoO^+, ZrO/ZrO^+, and NbC/NbC^+ the $|\Delta J^+|$ changes were observed to be larger than 5.[21,24,33] This observation has been rationalized on the basis of the channel coupling mechanism, as described and discussed in previous works.[20,34−36] However, rigorous theoretical schemes for simulations of rotational resolved state-to-state PFI−PE spectra, such as those presented here, await further theoretical developments.

On the basis of unambiguous rotational analyses and spectral simulation of the cleanly rotational revolved VIS−UV−PFI−PE spectra of Figures 2 and 3, the IE(VO) is determined to be 58 380.0 ± 0.7 cm^{-1} or 7.238 20 ± 0.000 09 eV. This value has a smaller error limit compared to the previous measurement but is in agreement with the previous study after taking into account the experimental uncertainties.[7] Using the present IE(VO) value and the IE(V) = 54 413 ± 1 cm^{-1} available in the literature,[29,37] we have obtained the 0 K bond dissociation energy (D_0) difference for VO^+ and VO to be $D_0(V^+{-}O) - D_0(V{-}O) = IE(V) - IE(VO) = -3967 \pm 1\ cm^{-1}$. The latter value should be valuable for benchmarking state-of-the-art theoretical predictions for $D_0(V^+{-}O)$ and $D_0(V{-}O)$.

B. VIS−UV−PFI−PE Spectra for $VO^+(X^3\Sigma^-;\ v^+ = 1, J^+)$.

The top black spectrum shown in Figure 4 (Figure 5) is the VIS−UV−PFI−PE spectrum for $VO^+(X^3\Sigma^-;\ v^+ = 1, J^+)$ obtained by setting VIS ω_1 = 17 432.54 cm^{-1} (17 442.27 cm^{-1}) and scanning UV ω_2 in the range 41 958−42 062 cm^{-1} (41 972−42 052 cm^{-1}). The total energy, i.e., the sum of VIS ω_1 and UV ω_2, is in the range 59 390−59 504 cm^{-1}. Following the discussion above, the VIS−UV−PFI−PE spectrum of Figure 4 is expected to consist of six rotational PFI−PE transitions series, $F_i^+(J^+)\ (i = 1{-}3) \leftarrow F_3'(J' = 3.5)$, and $F_i^+(J^+)\ (i = 1{-}3) \leftarrow F_4'(J' = 4.5)$. The corresponding simulated

DOI: 10.1021/acs.jpca.5b09458
J. Phys. Chem. A XXXX, XXX, XXX−XXX

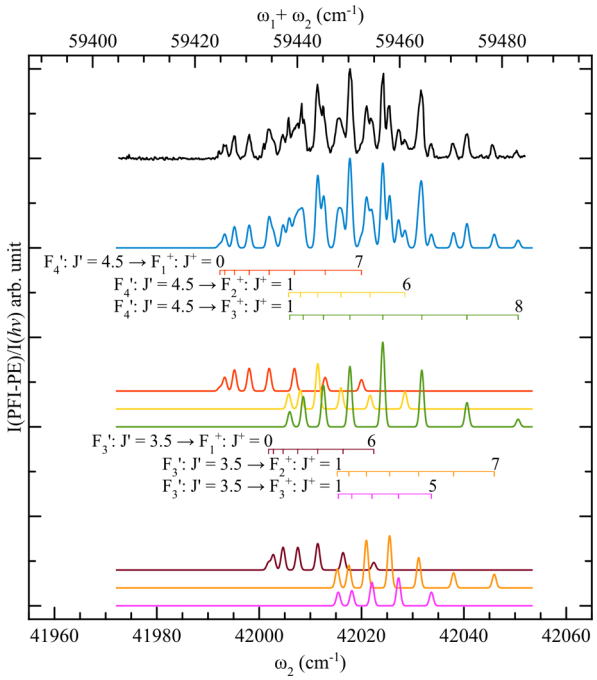

Figure 4. VIS−UV−PFI−PE spectrum for $VO^+(X^3\Sigma^-; v^+ = 1, J^+)$ (top black curve) obtained by setting VIS ω_1 = 17 432.54 cm^{-1} and scanning UV ω_2 in the range 41 972−42 052 cm^{-1}. At VIS ω_1 = 17 432.54 cm^{-1}, the $^TR_{31}(2.5)$ and $^TR_{42}(3.5)$ rotational transition lines of the $VO^*(C^4\Sigma^-; v' = 0) \leftarrow VO(X^4\Sigma^-; v'' = 0)$ band are excited, resulting in populating of the $VO^*[C^4\Sigma^-; v' = 0, F_3'(J' = 3.5)$ and $F_4'(J' = 4.5)]$ levels. The blue curve is the sum of individual simulations of the transition series, $VO^+[X^3\Sigma^-; v^+ = 1, F_i^+(J^+)$ $(i = 1-3)] \leftarrow VO^*[C^4\Sigma^-; v' = 0, F_3'(J' = 3.5)$ and $F_4'(J' = 4.5)]$, which are shown as the brown, orange, purple, red, yellow, and green curves, respectively.

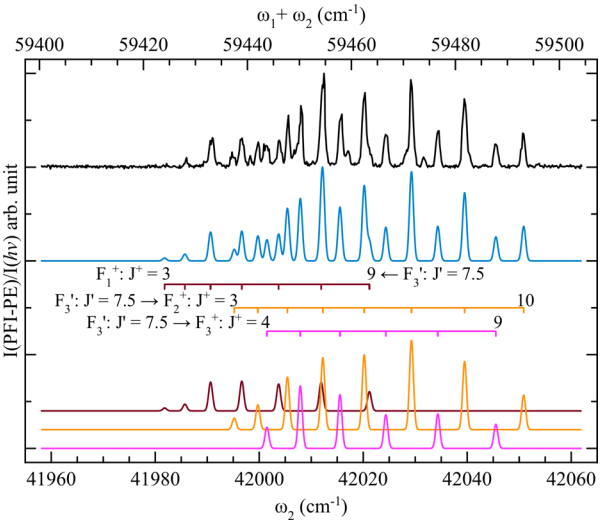

Figure 5. VIS−UV−PFI−PE spectrum for $VO^+(X^3\Sigma^-; v^+ = 1, J^+)$ (top black curve) obtained by fixing VIS ω_1 at 17 442.27 cm^{-1} and scanning UV ω_2 in the range 41 958−42 062 cm^{-1}. At VIS ω_1 = 17 442.27 cm^{-1}, the $^TR_{31}(6.5)$ transition of the $VO^*(C^4\Sigma^-; v' = 0) \leftarrow VO\ (X^4\Sigma^-; v'' = 0)$ band is excited, resulting in the population of $VO^*[C^4\Sigma^-; v' = 0, F_3(J' = 7.5)]$. The blue curve is the sum of individual simulated curves of the PFI−PE transitions, $VO^+[X^3\Sigma^-; v^+ = 1, F_i^+(J^+)$ $(i = 1-3] \leftarrow VO^*[C^4\Sigma^-; v' = 0, F_3'(J' = 7.5)]$, which are shown as the brown, orange, and purple curves, respectively.

spectra for these transition series are shown in Figure 4 as the brown, orange, purple, red, yellow, and green curves, respectively (bottom set of simulated spectra). The observation of the $J^+ = 0$ in $F_1^+(J^+)$ and $J^+ = 1$ in $F_2^+(J^+)$ and $F_3^+(J^+)$ indicates unambiguously that the term symmetry for the $VO^+(X)$ ground state is $^3\Sigma^-$. The VIS−UV−PFI−PE spectrum of Figure 5 consists of three rotational transition series, $F_i^+(J^+)$ $(i = 1-3) \leftarrow F_3'(J' = 7.5)$. The blue spectra shown below the PFI−PE spectra in Figures 4 and 5 represent the overall simulated spectra obtained by summing the individual simulated curves. The spectral analysis and simulation based on the pgopher software[30] give: ν_{10}^+ = 59 441.8 ± 0.7 cm^{-1}, B_1^+ = 0.5680 ± 0.0007 cm^{-1}, λ_1^+ = 6.702 ± 0.034 cm^{-1}, and γ_1^+ = 0.0303 ± 0.0059 cm^{-1}. The corresponding bond length derived from B_1^+ is r_1^+ = 1.561 ± 0.001 Å. The vibrational energies determined here for $VO^+(X^3\Sigma^-; v^+ = 0$ and 1) have allowed the determination of the vibration spacing to be $\Delta G(1/2)$ = 10 57.0 ± 0.7 cm^{-1}. These spectroscopic constants for $VO^+(X^3\Sigma^-; v^+ = 1)$ are included in Table 1.

C. VIS−UV−PFI−PE Spectra for $VO^+(X^3\Sigma^-; v^+ = 2, J^+)$.

The determination of the vibration spacing between the $v^+ = 0$ and 1 vibrational states has helped the successful search for higher excited v^+ states for $VO^+(X^3\Sigma^-)$ by VIS−UV−PFI−PE measurements. The top black spectrum of Figure 6 (Figure 7) depicts the VIS−UV−PFI−PE spectrum for $VO^+(X^3\Sigma^-; v^+ = 2, J^+)$ obtained by fixing ω_1 at 17 432.54 cm^{-1} (17 442.27 cm^{-1}) and scanning ω_2 in the range 43 022−43 104 cm^{-1} (43 013−43 114 cm^{-1}). The best overall simulated curve (blue

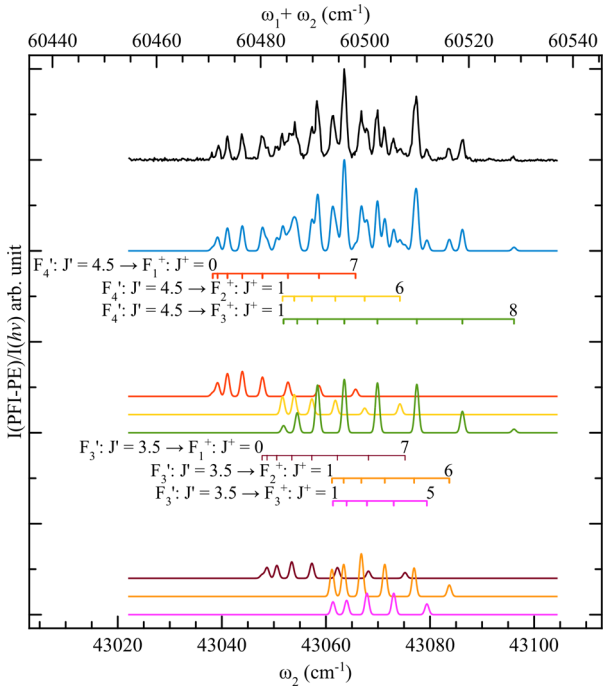

Figure 6. VIS−UV−PFI−PE spectrum for $VO^+(X^3\Sigma^-; v^+ = 2, J^+)$ (top black curve) obtained by setting VIS ω_1 at 17 432.54 cm^{-1} and scanning UV ω_2 in the range 43 022−43 104 cm^{-1}. At VIS ω_1 = 17 432.54 cm^{-1}, the $^TR_{31}(2.5)$ and $^TR_{42}(3.5)$ transitions of the $VO^*(C^4\Sigma^-; v' = 0) \leftarrow VO(X^4\Sigma^-; v'' = 0)$ band are excited, resulting in the population of the $VO^*[C^4\Sigma^-; v' = 0, F_3'(J' = 3.5)$ and $F_4'(J' = 4.5)]$ levels. The blue curve is the sum of individual simulations of the PFI−PE transitions, $VO^+[X^3\Sigma^-; v^+ = 2, F_i^+(J^+)$ $(i = 1-3)] \leftarrow VO^*[C^4\Sigma^-; v' = 0, F_3'(J' = 3.5)$ and $F_4'(J' = 4.5)]$, which are shown as brown, orange, purple, red, yellow and green, respectively.

DOI: 10.1021/acs.jpca.5b09458
J. Phys. Chem. A XXXX, XXX, XXX−XXX

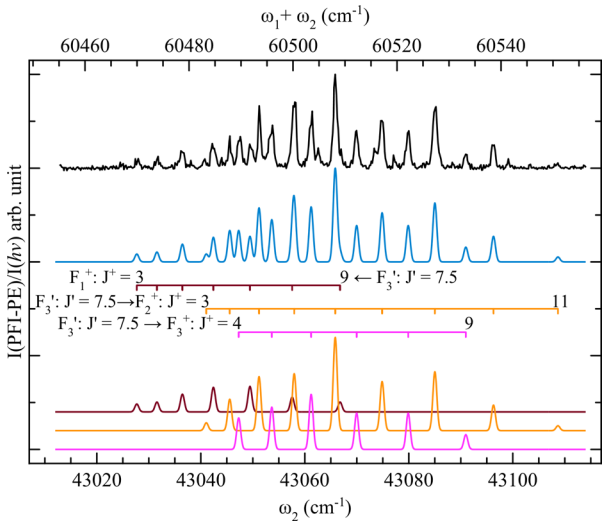

Figure 7. VIS−UV−PFI−PE spectrum for $VO^+(X^3\Sigma^-; v^+ = 2, J^+)$ (top black curve) obtained by setting VIS ω_1 at 17 442.27 cm^{-1} and scanning UV ω_2 in the range 43 013−43 114 cm^{-1}. At VIS ω_1 = 17 442.27 cm^{-1}, the $^TR_{31}(6.5)$ transition of the $VO^*(C^4\Sigma^-; v' = 0) \leftarrow VO(X^4\Sigma^-; v'' = 0)$ band is excited, resulting in the population of the $VO^*[C^4\Sigma^-; v' = 0, F_3(J' = 7.5)]$ level. The blue curve is the sum of individual simulated of the PFI−PE rotational transition series, $VO^+[X^3\Sigma^-; v^+ = 2, F_i^+(J^+)$ $(i = 1-3)] \leftarrow VO^*[C^4\Sigma^-; v' = 0, F_3'(J' = 7.5)]$, which are shown as the brown, orange, and purple curves, respectively.

316 spectrum) of the VIS−UV−PFI−PE spectrum of Figure 6 also
317 shows contributions of the six rotational transition series,
318 $F_i^+(J^+)$ $(i = 1-3) \leftarrow F_3'(J' = 3.5)$ and $F_i^+(J^+)$ $(i = 1-3) \leftarrow$
319 $F_4'(J' = 4.5)$, which are depicted as the brown, orange, purple,
320 red, yellow, and green curves, respectively (bottom set of
321 simulated curves). The assignment of $^3\Sigma^-$ is again confirmed by
322 the observation of $J^+ = 0$ in $F_1^+(J^+)$ and $J^+ = 1$ in $F_2^+(J^+)$ and
323 $F_3^+(J^+)$. The brown, orange, and purple curves shown in Figure
324 7 are the respective simulated spectra of the rotational
325 transition series, $F_i^+(J^+)$ $(i = 1-3) \leftarrow F_3(J' = 7.5)$ transition.
326 Again, the blue curve represents the overall simulated spectrum
327 obtained by summing the individual simulated curves for the
328 rotational series. The rotational pgopher[30] analysis and spectral
329 simulation of the PFI−PE spectra of Figures 6 and 7 yield the
330 spectroscopic constants for $VO^+(X^3\Sigma^-; v^+ = 2)$: $\nu_{20}^+ = 60\,487.7$
331 ± 0.7 cm^{-1}, $B_2^+ = 0.5636 \pm 0.0007$ cm^{-1}, $\lambda_2^+ = 6.690 \pm 0.035$
332 cm^{-1}, and $\gamma_2^+ = 0.0293 \pm 0.0065$ cm^{-1}. The B_2^+ constant gives
333 the bond length for $VO^+(X^3\Sigma^-; v^+ = 2)$ to be $r_2^+ = 1.568 \pm$
334 0.001 Å. These spectroscopic values for $VO^+(X^3\Sigma^-; v^+ = 2)$ are
335 also included in Table 1.

336 **D. VIS−UV−PFI−PE Spectra for $VO^+(X^3\Sigma^-; v^+ = 3, J^+)$.**
f8f9 337 Figure 8 (Figure 9) depicts the VIS−UV−PFI−PE spectrum
338 for $VO^+(X^3\Sigma^-; v^+ = 3, J^+)$ obtained by setting VIS ω_1 =
339 17 432.54 cm^{-1} (17 442.27 cm^{-1}) and scanning UV ω_2 in the
340 range 44 046−44 137 cm^{-1} (44 046−44 141 cm^{-1}). The overall
341 simulated curve (blue spectrum) depicted in Figure 8 is shown
342 to have contributions from the simulated PFI−PE spectra of six
343 rotational transition series: $F_i^+(J^+)$ $(i = 1-3) \leftarrow F_3'(J' = 3.5)$,
344 and $F_i^+(J^+)$ $(i = 1-3) \leftarrow F_4'(J' = 4.5)$, which are plotted as the
345 brown, orange, purple, red, yellow, and green curves,
346 respectively. The individual simulated curves of Figure 9 are
347 depicted as the brown curve for $F_1^+(J^+) \leftarrow F_3'(J' = 7.5)$, the
348 orange curve for $F_2^+(J^+) \leftarrow F_3'(J' = 7.5)$, and the purple curve
349 for $F_3^+(J^+) \leftarrow F_3'(J' = 7.5)$ transition series. The blue curve in

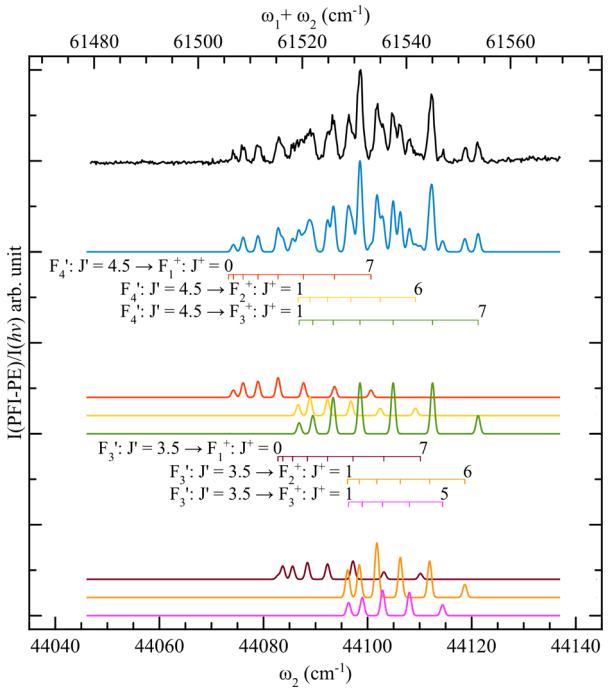

Figure 8. VIS−UV−PFI−PE spectrum for $VO^+(X^3\Sigma^-; v^+ = 3, J^+)$ (top black curve) obtained by setting VIS ω_1 at 17 432.54 cm^{-1} and scanning UV ω_2 in the range 44 046−44 137 cm^{-1}. At VIS ω_1 = 17 432.54 cm^{-1}, the $^TR_{31}(2.5)$ and $^TR_{42}(3.5)$ transitions of the $VO^*(C^4\Sigma^-; v' = 0) \leftarrow VO(X^4\Sigma^-; v'' = 0)$ band are excited, resulting in the population of the $VO^*[C^4\Sigma^-; v' = 0, F_3'(J' = 3.5)$ and $F_4'(J' = 4.5)]$ levels. The blue curve is the sum of individual simulations of the PFI−PE rotational transition series, $VO^+[X^3\Sigma^-; v^+ = 3, F_i^+(J^+)$ $(i = 1-3)] \leftarrow VO^*[C^4\Sigma^-; v' = 0, F_3(J' = 3.5)$ and $F_4'(J' = 4.5)]$, which are shown as the brown, orange, purple, red, yellow. and green curves, respectively.

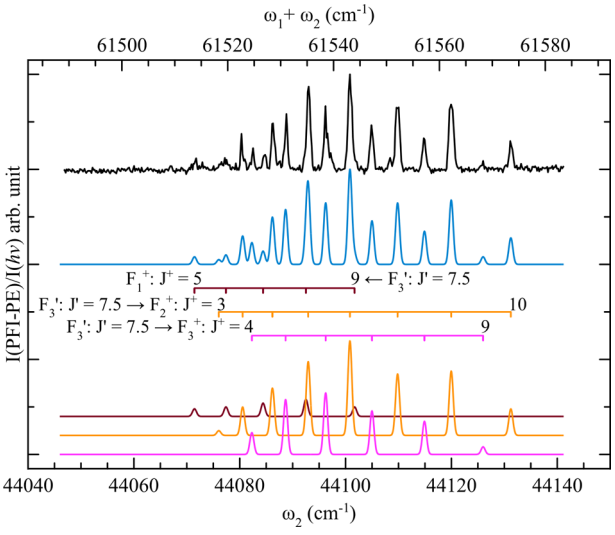

Figure 9. VIS−UV−PFI−PE spectrum for $VO^+(X^3\Sigma^-; v^+ = 3, J^+)$ (top black curve) obtained by setting VIS ω_1 at 17 442.27 cm^{-1} and scanning UV ω_2 in the range 44 046−44 141 cm^{-1}. At VIS ω_1 = 17 442.27 cm^{-1}, the $^TR_{31}(6.5)$ and transition of the $VO^*(C^4\Sigma^-; v' = 0) \leftarrow VO(X^4\Sigma^-; v'' = 0)$ band is excited, resulting in the population of the $VO^*[C^4\Sigma^-; v' = 0, F_3'(J' = 7.5)]$ level. The blue curve is the sum of individual simulations of the PFI−PE transitions $VO^+[X^3\Sigma^-; v^+ = 3, F_i^+(J^+)$ $(i = 0-3)] \leftarrow VO^*[C^4\Sigma^-; v' = 0, F_3'(J' = 7.5)]$, which are shown as the brown, orange, and purple curves, respectively.

DOI: 10.1021/acs.jpca.5b09458
J. Phys. Chem. A XXXX, XXX, XXX−XXX

Figure 9 is the sum of simulated curves for individual rotational transition series. The analysis and simulation of the experimental PFI–PE spectra based on the pgopher software[30] yields the spectroscopic constants: ν_{30}^{+} = 61 522.7 ± 0.7 cm^{-1}, B_3^+ = 0.5631 ± 0.0007 cm^{-1}, λ_3^+ = 6.675 ± 0.035 cm^{-1}, and γ_3^+ = 0.0209 ± 0.0065 cm^{-1} for $VO^+(X^3\Sigma^-; v^+= 3)$. The bond length r_3^+ = 1.568 ± 0.001 Å for $VO^+(X^3\Sigma^-; v^+= 3)$ is deduced from B_3^+. These spectroscopic values for $VO^+(X^3\Sigma^-; v^+= 3)$ are listed in Table 1 for comparison with values determined for other v^+ vibrational states.

Based on the band origins, ν_{00}^{+}, ν_{10}^{+}, ν_{20}^{+}, and ν_{30}^{+}, determined in the present study, the vibration spacings, $\Delta G(1/2)$, $\Delta G(3/2)$, and $\Delta G(5/2)$ for $VO^+(X^3\Sigma^-)$, are determined to be 1057.0 ± 0.7, 1045.9 ± 0.7, and 1035.0 ± 0.7 cm^{-1}, respectively. By using the standard equations of eqs 2 and 3,

$$\Delta G(v^+ + 1/2) = G(v^+ + 1) - G(v^+) \quad (2)$$

$$G(v^+) = \omega_e^+(v^+ + (1/2)) - \omega_e^+ x_e^+(v^+ + (1/2))^2 \quad (3)$$

we have determined the vibration constants for $VO^+(X^3\Sigma^-)$ to be ω_e^+ = 1068.0 ± 0.7 cm^{-1}, and $\omega_e^+\chi_e^+$ = 5.5 ± 0.7 cm^{-1}.

Furthermore, by solving the standard equation

$$B_v^+ = B_e^+ - \alpha_e^+(v^+ + (1/2)) \quad (4)$$

with the values of B_0^+ = 0.5705 ± 0.0005 cm^{-1}, B_1^+ = 0.5680 ± 0.0007 cm^{-1}, B_2^+ = 0.5636 ± 0.0007 cm^{-1}, and B_3^+ = 0.5631 ± 0.0008 cm^{-1} obtained in this experiment, the rotation constants are determined to be B_e^+ = 0.5716 ± 0.0012 cm^{-1} and α_e^+ = 0.0027 ± 0.0005 cm^{-1}. The equilibrium bond length are derived to be r_e^+ = 1.557 ± 0.002 Å. All energetic and spectroscopic data determined in the present experiment are summarized in Table 1 for comparison with available experimental data for $VO^+(X^3\Sigma^-)$ available in the literature.

IV. CONCLUSIONS

The rotationally resolved state-to-state PFI–PE spectra for $VO^+(X^3\Sigma^-, v^+ = 0, 1, 2, \text{and } 3)$ have been obtained by the two-color VIS–UV–PFI–PE method. The rotationally selected and resolved spectra thus obtained have confirmed that the $VO^+(X)$ ground state has the term symmetry of $^3\Sigma^-$. The rotational analysis yields the rotational constant B_e^+ = 0.5716 ± 0.0012 cm^{-1} and α_e^+ = 0.0027 ± 0.0005 cm^{-1}. The equilibrium bond length determined from this B_e value is r_e^+ = 1.557 ± 0.002 Å. The unambiguous rotational assignment has allowed the determination of a more precise IE(VO) value to be 58 380.0 ± 0.7 cm^{-1} or 7.238 20 ± 0.000 09 eV. The VIS–UV–PFI–PE measurements for the vibrationally excited levels $VO^+(X^3\Sigma^-, v^+ = 1, 2, \text{and } 3)$ have allowed the determination of the vibration constants, ω_e^+ = 1068.0 ± 0.7 cm^{-1} and $\omega_e^+ x_e^+$ = 5.5 ± 0.7 cm^{-1}. The 0 K bond dissociation energy difference, $D_0(V^+–O) - D_0(V–O)$, is also determined to be −3967 ± 1 cm^{-1}. The latter value is expected to be useful for benchmarking theoretical predictions of $D_0(V^+–O)$ and $D_0(V–O)$.

AUTHOR INFORMATION

Corresponding Author

*C. Y. Ng. E-mail address: cyng@ucdavis.edu.

Notes

The authors declare no competing financial interest.

ACKNOWLEDGMENTS

This material is based upon work supported by the National Science Foundation under CHE-0910488 and CHE-1462172.

REFERENCES

(1) Brett, J. M. Astrophysical Oscillator Strengths for Tio and Vo Bands from Spectrum Synthesis of Spectral Types M1 Iii to M7 Iii. *Astron. Astrophys.* **1990**, *231*, 440–452.

(2) Cheung, A.-C.; Hansen, R. C.; Merer, A. J. Laser Spectroscopy of Vo: Analysis of the Rotational and Hyperfine Structure of the $C^4\Sigma^-$-$X^4\Sigma^-$ (0,0) Band. *J. Mol. Spectrosc.* **1982**, *91*, 165–208.

(3) Dyke, J. M.; Gravenor, B. W. J.; Hastings, M. P.; Morris, A. High-Temperature Photoelectron Spectroscopy: The Vanadium Monoxide Molecule. *J. Phys. Chem.* **1985**, *89*, 4613–4617.

(4) Aristov, N.; Armentrout, P. B. Collision-Induced Dissociation of Vanadium Monoxide Ion. *J. Phys. Chem.* **1986**, *90*, 5135–5140.

(5) Merer, A. J.; Huang, G.; Cheung, A.-C.; Taylor, A. W. New Quartet and Doublet Electronic Transitions in the near-Infrared Emission Spectrum of VO. *J. Mol. Spectrosc.* **1987**, *125*, 465–503.

(6) Clemmer, D.; Elkind, J.; Aristov, N.; Armentrout, P. Reaction of Sc^+, Ti^+, and V^+ with CO. Mc^+ and Mo^+ Bond Energies. *J. Chem. Phys.* **1991**, *95*, 3387.

(7) Harrington, J.; Weisshaar, J. C. State-to-State Photoionization of VO: Propensity for Large, Positive Changes in Rotational Quantum Number. *J. Chem. Phys.* **1992**, *97*, 2809–2812.

(8) Wu, H. B.; Wang, L.-S. A Photoelectron Spectroscopic Study of Monovanadium Oxide Anions (VO^{x-}, X= 1–4). *J. Chem. Phys.* **1998**, *108*, 5310–5318.

(9) Ram, R. S.; Bernath, P. F.; Davis, S. P.; Merer, A. J. Fourier Transform Emission Spectroscopy of a New $^2\Phi$–$1\ ^2\Delta$ System of VO. *J. Mol. Spectrosc.* **2002**, *211*, 279–283.

(10) Ram, R. S.; Bernath, P. F. Emission Spectroscopy of a New $^2\Delta$–$1\ ^2\Delta$ System of VO. *J. Mol. Spectrosc.* **2005**, *229*, 57–62.

(11) Pykavy, M.; van Wüllen, C. Multireference Correlation Calculations for the Ground States of $VO^{+/0/-}$Using Correlation Consistent Basis Sets. *J. Phys. Chem. A* **2003**, *107*, 5566–5572.

(12) Jakubikova, E.; Rappé, A. K.; Bernstein, E. R. Density Functional Theory Study of Small Vanadium Oxide Clusters. *J. Phys. Chem. A* **2007**, *111*, 12938–12943.

(13) Miliordos, E.; Mavridis, A. Electronic Structure of Vanadium Oxide. Neutral and Charged Species, $VO^{0,\pm}$. *J. Phys. Chem. A* **2007**, *111*, 1953–1965.

(14) Bande, A.; Lüchow, A. Vanadium Oxide Compounds with Quantum Monte Carlo. *Phys. Chem. Chem. Phys.* **2008**, *10*, 3371–3376.

(15) Chang, Y. C.; Lam, C. S.; Reed, B.; Lau, K. C.; Liou, H.; Ng, C. Rovibronically Selected and Resolved Two-Color Laser Photoionization and Photoelectron Study of the Iron Carbide Cation. *J. Phys. Chem. A* **2009**, *113*, 4242–4248.

(16) Chang, Y. C.; Shi, X.; Lau, K. C.; Yin, Q. Z.; Liou, H.; Ng, C. Rovibronically Selected and Resolved Two-Color Laser Photoionization and Photoelectron Study of Nickel Carbide Cation. *J. Chem. Phys.* **2010**, *133*, 054310.

(17) Huang, H.; Chang, Y. C.; Luo, Z.; Shi, X.; Lam, C.-S.; Lau, K.-C.; Ng, C. Rovibronically Selected and Resolved Two-Color Laser Photoionization and Photoelectron Study of Cobalt Carbide Cation. *J. Chem. Phys.* **2013**, *138*, 094301.

(18) Huang, H.; Luo, Z.; Chang, Y. C.; Lau, K.-C.; Ng, C. Rovibronically Selected and Resolved Two-Color Laser Photoionization and Photoelectron Study of Titanium Monoxide Cation. *J. Chem. Phys.* **2013**, *138*, 174309.

(19) Huang, H.; Luo, Z. h.; Chang, Y. C.; Lau, K. C.; Ng, C. Y. State-to-State Photoionization Dynamics of Vanadium Nitride by Two-Color Laser Photoionization and Photoelectron Methods. *Chin. J. Chem. Phys.* **2013**, *26*, 669–678.

(20) Luo, Z.; Huang, H.; Chang, Y.-C.; Zhang, Z.; Yin, Q.-Z.; Ng, C. Y. Rotationally Resolved State-to-State Photoionization and Photo-

DOI: 10.1021/acs.jpca.5b09458
J. Phys. Chem. A XXXX, XXX, XXX–XXX

electron Study of Titanium Carbide and Its Cation (TiC/TiC$^+$). *J. Chem. Phys.* **2014**, *141*, 144307.
(21) Luo, Z.; Huang, H.; Zhang, Z.; Chang, Y. C.; Ng, C. Y. Rotationally Resolved State-to-State Photoelectron Study of Niobium Carbide Radical. *J. Chem. Phys.* **2014**, *141*, 024304.
(22) Ng, C.-Y. State-to-State Spectroscopy and Dynamics of Ions and Neutrals by Photoionization and Photoelectron Methods. *Annu. Rev. Phys. Chem.* **2014**, *65*, 197−224.
(23) Chang, Y. C.; Luo, Z.; Pan, Y.; Zhang, Z.; Song, Y.-N.; Kuang, S. Y.; Yin, Q. Z.; Lau, K.-C.; Ng, C. Y. Rotationally Resolved State-to-State Photoionization and the Photoelectron Study of Vanadium Monocarbide and Its Cations (VC/VC$^+$). *Phys. Chem. Chem. Phys.* **2015**, *17*, 9780−9793.
(24) Luo, Z.; Chang, Y.-C.; Zhang, Z.; Ng, C. Y. Rotationally Resolved State-to-State Photoelectron Study of Zirconium Monoxide Cation (ZrO$^+$). *Mol. Phys.* **2015**, *113*, 2228−2242.
(25) Luo, Z.; Zhang, Z.; Huang, H.; Chang, Y. C.; Ng, C. Y. State-to-State Photoionization and Photoelectron Study of Vanadium Methylidyne Radical. *J. Chem. Phys.* **2014**, *140*, 181101.
(26) Chang, Y.-C.; Huang, H.; Luo, Z.; Ng, C. Communication: A Vibrational Study of Titanium Dioxide Cation Using the Vacuum Ultraviolet Laser Pulsed Field Ionization-Photoelectron Method. *J. Chem. Phys.* **2013**, *138*, 041101.
(27) Lau, K. C.; Chang, Y. C.; Lam, C. S.; Ng, C. High-Level Ab Initio Predictions for the Ionization Energy, Bond Dissociation Energies, and Heats of Formations of Iron Carbide (FeC) and Its Cation (FeC$^+$). *J. Phys. Chem. A* **2009**, *113*, 14321−14328.
(28) Lau, K.-C.; Chang, Y. C.; Shi, X.; Ng, C. Y. High-Level Ab Initio Predictions for the Ionization Energy, Bond Dissociation Energies, and Heats of Formation of Nickel Carbide (NiC) and Its Cation (NiC). *J. Chem. Phys.* **2010**, *133*, 114304.
(29) Lau, K.-C.; Pan, Y.; Lam, C.-S.; Huang, H.; Chang, Y.-C.; Luo, Z.; Shi, X.; Ng, C. Y. High-Level Ab Initio Predictions for the Ionization Energy, Bond Dissociation Energies, and Heats of Formation of Cobalt Carbide (CoC) and Its Cation (CoC$^+$). *J. Chem. Phys.* **2013**, *138*, 094302.
(30) PGOPHER, a Program for Simulating Rotational Structure, Western, C. M., University of Bristol, http://dx.doi.org/10.5523/bris.huflggvpcuc1zvliqed497r2.
(31) Wang, P.; Xing, X.; Lau, K. C.; Woo, H. K.; Ng, C.-Y. Rovibrational-State-Selected Pulsed Field Ionization-Photoelectron Study of Methyl Iodide Using Two-Color Infrared-Vacuum Ultraviolet Lasers. *J. Chem. Phys.* **2004**, *121*, 7049−7052.
(32) Xing, Xi; Reed, Beth; Bahng, Mi-Kyung; Baek, S.-J.; Wang, Peng; Ng, C. Y. Infrared−Vacuum Ultraviolet−Pulsed Field Ionization−Photoelectron Study of CH_3I^+ Using a High-Resolution Infrared Laser. *J. Chem. Phys.* **2008**, *128*, 104306.
(33) Luo, Z.; Chang, Y.-C.; Pan, Y.; Lau, K.-C.; Ng, C. Y. Rotationally Resolved State-to-State Photoelectron Study of Molybdenum Monoxide Cation (MoO$^+$). *J. Phys. Chem. A* **2015**, DOI: 10.1021/acs.jpca.5b07939.
(34) Merkt, F.; Softley, T. P. Rotational Line Intensities in Zero Kinetic Energy Photoelectron Spectroscopy (Zeke-Pes). *Int. Rev. Phys. Chem.* **1993**, *12*, 205−239.
(35) Schlag, E. W. *Zeke Spectroscopy*; Cambridge University Press: Cambridge, U.K., 1996.
(36) Linton, C.; Simard, B.; Loock, H. P.; Wallin, S.; Rothschopf, G. K.; Gunion, R. F.; Morse, M. D.; Armentrout, P. B. Rydberg and Pulsed Field Ionization-Zero Electron Kinetic Energy Spectra of YO. *J. Chem. Phys.* **1999**, *111*, 5017.
(37) Page, R. H.; Gudeman, C. S. Completing the Iron Period: Double-Resonance, Fluorescence-Dip Rydberg Spectroscopy and Ionization Potentials of Titanium, Vanadium, Iron, Cobalt, and Nickel. *J. Opt. Soc. Am. B* **1990**, *7*, 1761−1771.

DOI: 10.1021/acs.jpca.5b09458
J. Phys. Chem. A XXXX, XXX, XXX−XXX